

Direct Observation of Adsorption Morphologies of Cationic Surfactants at the Gold Metal–Liquid Interface

Md. Rubel Khan, Himanshu Singh, Sumit Sharma, and Katherine Leslee Asetre Cimatu*



Cite This: *J. Phys. Chem. Lett.* 2020, 11, 9901–9906



Read Online

ACCESS |

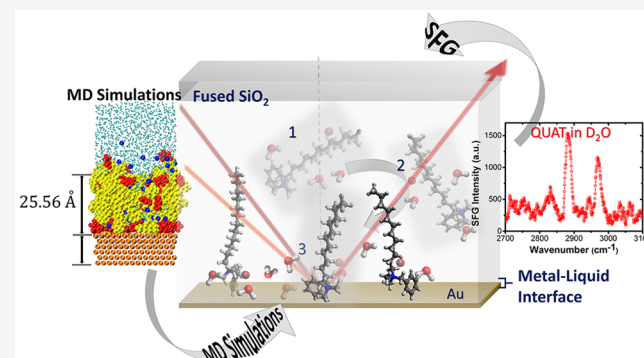
Metrics & More

Article Recommendations

Supporting Information

ABSTRACT: Understanding interfacial phenomena is important in processes like corrosion, catalysis, and electrochemical reactions. Specifically, in corrosion inhibition, the assembly of adsorbed surfactants at metal–water interfaces in well-packed, ordered layers is desired. We provide direct evidence of the role of alkyl tails of surfactants in the formation of ordered adsorbed layers at metal–water interfaces. We have employed surface-specific sum frequency generation (SFG) spectroscopy to probe the *in situ* adsorption and self-assembly of cationic surfactants, alkyltrimethylbenzyl ammonium bromides of tail lengths $n = 4$ (C4) and 12 (C12), without any applied potential or stimulus, at the gold–water interface. Our SFG measurements show that C12 Quat adsorbs as an ordered monolayer, whereas C4 Quat adsorbs in a disordered monolayer.

All-atom molecular dynamics (MD) simulations of these surfactants corroborate with SFG results. These findings provide new insights on how hydrophobic interactions between alkyl tails of surfactants affect their self-assembly at metal–water interfaces.



Internal corrosion of oil-and-gas pipelines is a major health, safety, and environmental problem that is estimated to cost roughly \$7 billion/yr in the United States alone.¹ Corrosion inhibitors are surfactant molecules that are injected in the oil-and-gas pipelines to retard corrosion.² Surfactants are amphiphilic compounds. Due to their chemical structure, surfactants tend to adsorb onto solid metal surfaces from aqueous solution. These surfactants are understood to create a hydrophobic barrier for corrosive substances like carbon dioxide (CO_2), hydrogen sulfide (H_2S), and water (H_2O), which slows the rate of corrosion.^{3,4} For effective corrosion inhibition, it is desired that the alkyl tails of adsorbed surfactants form a well-packed, ordered layer on the metal surface.⁵ This raises an important question as to how the alkyl tails affect the adsorption morphologies of the surfactants. Previous studies of the adsorption of anionic and cationic surfactants on metal oxide surfaces suggest that the initial adsorption is driven by the affinity between the charged head groups of the surfactants and the surfaces upon application of a stimulus (concentration and pH changes).^{6,7} Atomic force microscopy and surface-enhanced Raman spectroscopy have also revealed the presence of ordered layers of adsorbed surfactants on metal surfaces, which suggests that hydrophobic interactions between the alkyl tails play a role in the adsorption process.^{8,9} However, there has not been any direct measurement of the molecular configurations in the adsorbed layers. Other studies have examined the adsorption behavior of monolayers on a metal surface at the air–solid and liquid–solid interfaces facilitated by an applied potential.^{10–14}

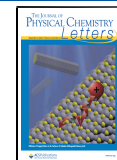
However, the spontaneous adsorption of surfactants from aqueous solution to the metal surface without external stimuli has not been investigated as yet.

In this report, for the first time, the *in situ* adsorption of cationic surfactants (Quats) and their assembly, in ordered morphologies without any assisting mechanism studied via SFG spectroscopy, has been reported. SFG has been employed previously to observe preadsorbed monolayers before exposure to a liquid environment under electrochemical conditions^{15,16} and to also directly observe corrosion and electrochemical reduction products at the metal–liquid interface.^{17,18} Observing *in situ* organization of surfactants on metal surfaces is challenging and predicting the adsorption behavior is difficult because of the many interactions that are involved in the adsorption process. We have studied the adsorption and self-assembly of C4 and C12 Quat surfactants using SFG to also understand the effect of the length of alkyl tails on the adsorption behavior. In this study, we present direct measurements of molecular-level details of the adsorbed layers of C4 and C12. Along with SFG, we have also performed fully

Received: August 18, 2020

Accepted: October 30, 2020

Published: November 10, 2020



atomistic simulations of C4 and C12 at the gold–water interface.

SFG spectroscopy is an interface-selective technique that has been popularly used to obtain vibrational spectra of monolayers formed on metal and dielectric surfaces at a molecular level.^{13,19–21} The spectral analysis provides information about conformation, chemical identification, orientation, and dynamics of adsorbed interfacial molecules.^{22,23} The details of SFG theory and setup have been described elsewhere.^{21–26}

The adsorption behavior of alkyldimethylbenzylammonium bromide (Quat) of two different tail lengths ($n = 4$ and $n = 12$, henceforth referred to as C4 and C12, respectively) at the gold metal–liquid interface was investigated by SFG spectroscopy. The application of the SFG technique to the water–solid interface is experimentally challenging due to the strong absorption of the infrared beam by the water molecules along with the nonresonant background coming from the metal surface. Here, we probed this interface using the geometry shown in Figure 1 where the incident beams (visible and

infrared) passed through the fused silica window and the liquid to the metal surface. Then, the beams including the SFG beam were reflected from the metal surface through the liquid and the window. The solution was sandwiched using a $\sim 250\text{ }\mu\text{m}$ thickness Teflon spacer between the fused silica window and the metal surface. The thickness of the spacer is sufficient to reduce interference between the window and the gold metal surface and other experimental artifacts. The systematic suppression of the nonresonant contribution from the metal surface was achieved while maintaining the SFG spectral profile. This approach contributes toward expanding applications of SFG to study other phenomena at the metal–liquid interfaces. The details on data acquisition and fitting analysis, including the results for the determination of the average tilt angles, are available in the Supporting Information. The structure of the surfactant molecules and a schematic showing adsorption of C4 molecules from the solution scheme are shown in Figure 1.

C4 and C12 Quat solutions of concentration 0.4 mM in D₂O, which is below the critical micelle concentrations (CMCs) of both C4 and C12 Quat,²² were allowed to equilibrate for an hour inside the SFG cell. D₂O was used to avoid any interference from the OH vibrational modes in the analysis of the CH vibrational modes. The spectra were collected by suppressing the nonresonant contribution from the gold substrate.²⁷ The time delay for ssp and ppp polarization combinations were $\sim 2.40\text{ ps}$ and $\sim 3.00\text{ ps}$, respectively. The delays were determined by collecting the spectra at different times until the nonresonant background was sufficiently suppressed. An example of how this suppression was developed at different timing delays is shown in Figure S2 for C12 Quat. In Figure 2, the C4 Quat ssp spectrum (Figure 2(A)) contained a prominent methylene asymmetric stretch peak (CH₂ AS) at $\sim 2907\text{ cm}^{-1}$.^{28,29} The other CH stretches are less prominent (peak assignments and positions are reported in the SI).^{22,26,30,31} The methyl asymmetric stretch was not evident in the ssp spectrum compared to other vibrational modes, especially to the methylene groups that dominated the surface. In the C12 Quat ssp spectrum, sharp peaks of the terminal methyl symmetric (CH₃ SS) ($\sim 2884\text{ cm}^{-1}$) and methyl symmetric

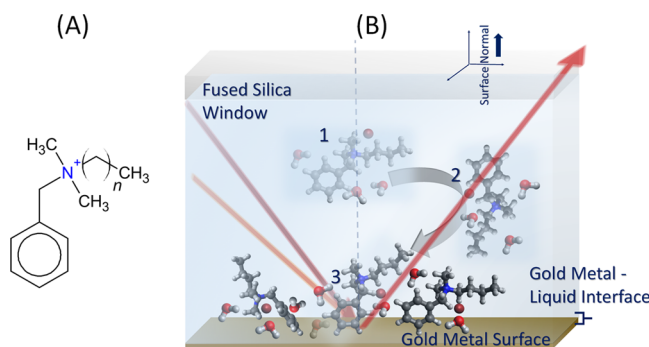


Figure 1. (A) Structure of quaternary ammonium-based surfactant molecules employed in this study. The subscript n indicates the number of CH₂ groups in the alkyl tail (where $n = 3$ and $n = 11$ carbon atoms are C4 and C12, respectively). (B) Schematic diagram of a C4 molecule's mechanism of adsorption from the (1 and 2) solution to the gold metal surface (3).

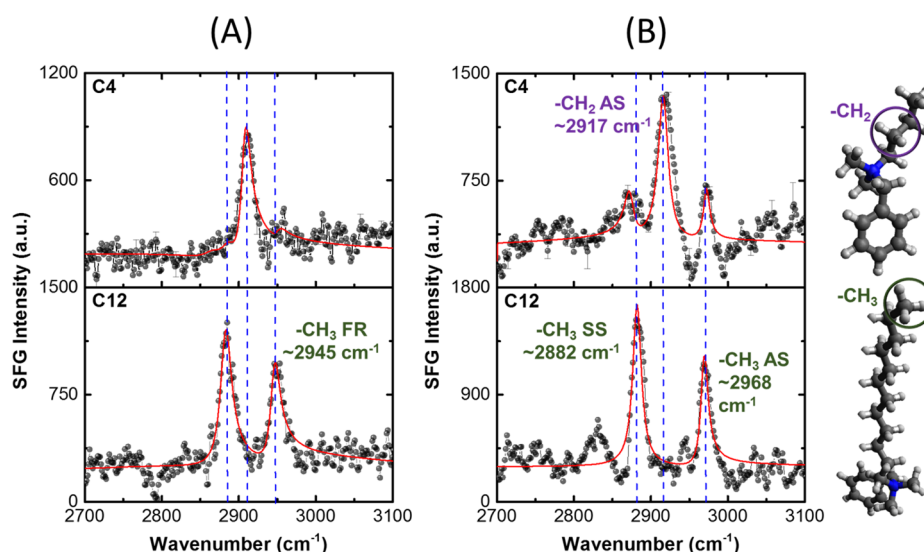


Figure 2. Fitted SFG spectra of 0.4 mM C4 and C12 Quat in D₂O at (A) ssp and (B) ppp polarization combinations.

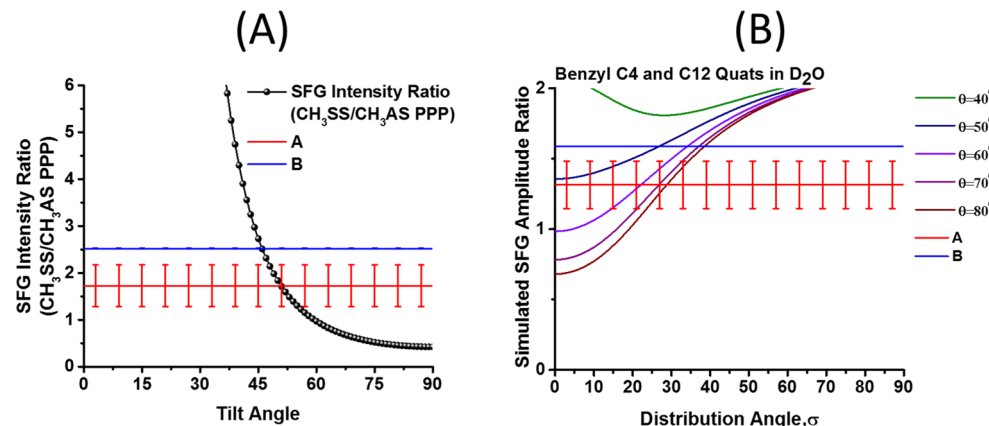


Figure 3. (A) The fitted SFG intensity ratios ($\text{CH}_3\text{SS}/\text{CH}_3\text{AS}$ PPP) are matched to the SFG simulated curves as a function of the tilt angle to estimate the average tilt angles, and (B) the fitted SFG amplitude ratios ($\text{CH}_3\text{SS}/\text{CH}_3\text{AS}$ PPP) are also matched to the SFG simulated curves as a function of the distribution angle (σ) to estimate the distribution of tilt angles for C4 and C12 Quat molecules. The percent errors are calculated at a 95% confidence limit.^{22,26,27,34,38,39}

stretch split by the Fermi resonance interaction with the methyl bending mode (CH_3 FR) ($\sim 2945\text{ cm}^{-1}$) are observed.^{31,32} In the C4 Quat PPP spectrum (Figure 2(B)), CH_3SS , CH_2AS , and methylene asymmetric stretch (CH_3AS) vibrational modes are observed at ~ 2880 , ~ 2917 , and $\sim 2972\text{ cm}^{-1}$, respectively.^{30,31,33} In addition, the CH_3AS present is more evident in the PPP spectrum while it is not evident in the SSP spectrum; the possible reason for this observation can be because most of the AS vibrational modes are not aligned along with the s-polarized lights of the visible and SF beams in the SSP polarization. The CH_3AS is otherwise evident in the PPP spectrum. As the polarization of both incident beams is parallel to the incident plane (p-polarized), AS stretches are probed by the p-polarized visible and IR beams while only p-polarized SFG signal is recorded. This could be because CH_3AS vibrational modes lie parallel to the incident plane.^{34,35} On the other hand, peaks of the CH_3SS and CH_3AS peaks are observed and prominent in the C12 Quat PPP spectrum.^{30,32,33} Tables S3 and S4 summarize the peak positions from fittings and assignments, which are available in the SI.

The C12 spectrum in Figure 2 is dominated by CH_3 vibrational modes while the CH_2 modes are barely noticeable. This observation indicates that the C12 alkyl tail is ordered because the tails are arranged in *trans* conformation. As a result, the tails have a close-packed arrangement due to the increased hydrophobic tail-tail interaction and initial adsorption driven by the affinity of the charged headgroup to the gold metal surface.^{6,7,36} In contrast, the C4 spectrum is dominated by the CH_2 mode and the CH_3 modes are less visible. This observation indicates that the C4 alkyl tail is less ordered, resulting in a random orientation and more gauche defects due to weaker hydrophobic interactions between the shorter tails.³⁷ However, Coulombic interactions between the C4 surfactant and the metal surface are still significant enough that the C4 Quat surfactant is observed at the gold metal-liquid interface. Also, the average tilt angle (θ) values of the methyl (CH_3) terminal group of C4 and C12 Quat (Figure 3) were estimated from the fitted data.²⁶ The θ is the angle of the terminal methyl group from the surface normal. The θ values were determined by taking the intensity ratios between the CH_3SS and CH_3AS from the fitted PPP spectra.^{22,26} Then, the intensity ratios must be intersected with the SFG simulated

curve to estimate the θ (Figure 3).²⁵ The θ values are $51^\circ \pm 13^\circ$ and $46^\circ \pm 0.1^\circ$ for C4 and C12, respectively. The θ values of C4 show a large standard deviation, indicating that the molecules are not ordered, unlike in the case of C12 molecules with a smaller deviation. On the other hand, a large deviation may also be due to the goodness of the fitting of the SFG raw spectra. The smaller deviation in the tilt angle of C12 is a consequence of stronger hydrophobic effects between the tails of the surfactants, which leads to an ordered structure. In addition, we are also reporting the distribution angles for both C4 and C12 Quat molecules. The distribution angles for C4 are $22^\circ \pm 3^\circ$ (60° tilt angle), $27^\circ \pm 3^\circ$ (70° tilt angle), and $29^\circ \pm 4^\circ$ (80° tilt angle), whereas for C12 we have the following values of $27^\circ \pm 0.03^\circ$ (50° tilt angle), $34^\circ \pm 0.04^\circ$ (60° tilt angle), $37^\circ \pm 0.04^\circ$ (70° tilt angle), and $38^\circ \pm 0.04^\circ$ (80° tilt angle). This also means that the distribution angles estimated for every tilt angle are narrow, ranging from 22° to 38° , which is less than 90° (defined as a broad distribution).^{22,26,34,38,39} Table S6 summarizes the average tilt angles and distribution angles for the methyl groups of C4 and C12 Quats.

The adsorbed configurations of C4 and C12 Quat molecules were studied via MD simulations. Following previous works,^{40,41} we initiated the simulations by organizing the surfactants in a SAM configuration at the gold metal-water interface (Figure S3). Canonical ensemble MD simulations were performed with a vapor space of 20 \AA to ensure that the system was maintained at saturation pressure.⁴² The simulations were run for $580\text{--}773\text{ ns}$. Equilibration was ensured by comparing the ensemble-averaged distribution of surfactants, water, and counterions of successive time periods of 40 ns . Details of the simulation setup are available in the Supporting Information. Figure 4 shows configurations of the C4 and C12 Quat molecules after the MD simulations.

A distribution of tilt angles is also computed from MD simulations and is shown in Figure S4. The average tilt angles are found to be $59.3^\circ \pm 1.4^\circ$ and $52.1^\circ \pm 1.0^\circ$ for the C4 and the C12 molecules, respectively. The values of average tilt angles obtained in the MD simulations are in qualitative agreement with the estimated average tilt angles from SFG spectroscopy.

Figure 5(A) shows the distribution of orientation of alkyl tails of the surfactants with respect to the surface normal, averaged over the last 120 ns of simulation. We have calculated

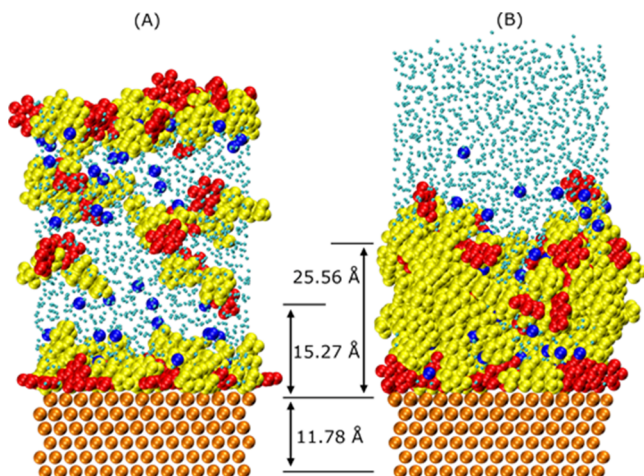


Figure 4. Snapshots of the configuration of (A) C4 molecules and (B) C12 molecules at $t = 677$ ns and $t = 500$ ns. Red beads represent the aromatic rings, and the yellow beads represent the alkyl tails. Water molecules are represented in cyan color, and the gold lattice is represented by orange beads. The blue beads represent bromides. The length of a C12 molecule is 15.27 Å.

the orientation of the alkyl tails by first defining the end-to-end vector as a vector joining the nitrogen atom of the polar head to the carbon atom of the terminal CH_3 group. The orientation profiles show that a fraction of C4 Quat molecules adsorbed with their molecular axis perpendicular to the surface normal. The distribution profile is calculated as $\frac{\langle H(\theta) \rangle}{\langle N \rangle \sin \theta}$ wherein $\langle H(\theta) \rangle$ is the ensemble-averaged histogram of the angle θ between the end-to-end vector of the adsorbed molecules and the surface normal and $\langle N \rangle$ is the ensemble-average number of adsorbed molecules. The distribution profile shows that C12 Quat molecules are predominantly aligned close to the surface normal. On the other hand, the distribution of C4 Quat molecules has a peak at $\sim 90^\circ$ and a distribution around 25° . This suggests that while the adsorbed C12 Quat molecules form an ordered configuration, the adsorption of C4 molecules is disordered. These MD results support the observations for C4 and C12 molecules using SFG.

Figure 5 (B) shows the distribution of the angle that the normal vector of the aromatic rings form with the surface normal. This distribution is also calculated as $\frac{\langle H(\theta) \rangle}{\langle N \rangle \sin \theta}$ where

$\langle H(\theta) \rangle$ is now the ensemble-averaged histogram of the angle between the normal vector of the aromatic rings of adsorbed molecules and the surface normal. A peak in the distribution at $\theta \approx 0^\circ$ implies that in the adsorbed state of both C4 and C12 Quat molecules, the aromatic rings predominantly lie flat on the surface. An important conclusion from these distributions is that the alkyl tails of C12 molecules mostly stand up on the surface. This is further confirmed from Figure S5, which shows the distribution of the angle between the alkyl tail and the normal vector to the aromatic ring of the adsorbed molecules. Analogous to Figure S5 is Figure S6, which shows the same distribution but for the molecules in the bulk aqueous phase. Most adsorbed C12 molecules are bent as compared to their conformation in the bulk phase. We have confirmed the validity of our simulation results by studying a larger simulation system with twice the surface area and the number of C12 molecules (Figure S10). Overall, our MD simulation results verify the experimental findings that the C12 molecules form a well-ordered adsorbed configuration, whereas the C4 molecules are adsorbed in random orientations. Also, the MD simulations reveal details about conformations of the adsorbed molecules in the ordered monolayer.

In summary, by performing interfacial analysis using sum frequency generation (SFG) spectroscopy, we have studied the unassisted adsorption behavior of surfactants onto the gold metal surface from aqueous solution. This study demonstrates that the *in situ* SFG spectroscopy is a powerful tool to probe the adsorption and self-assembly of cationic surfactants and perform orientational analysis at the liquid–solid interface. The longer alkyl tail surfactant (C12) formed an ordered monolayer onto the metal surface and has a *trans* conformation because of strong tail–tail interactions. However, the shorter alkyl tail surfactant (C4) formed a less ordered or randomly oriented monolayer on the metal surface due to the weak tail–tail interactions. We attribute these findings on tail lengths, conformation, and adsorption as key factors for SAM formation. Our simulation results corroborate with experiments, showing that the C4 molecules adsorb in random orientations, whereas the C12 molecules adsorb in a well-packed, ordered monolayer configuration. These fundamental findings will also lead to our future work on the adsorption of surfactants on the commercial-grade mild steel at different ionic strengths or salt concentrations with and without the applied potential to mimic the actual corrosive environment.

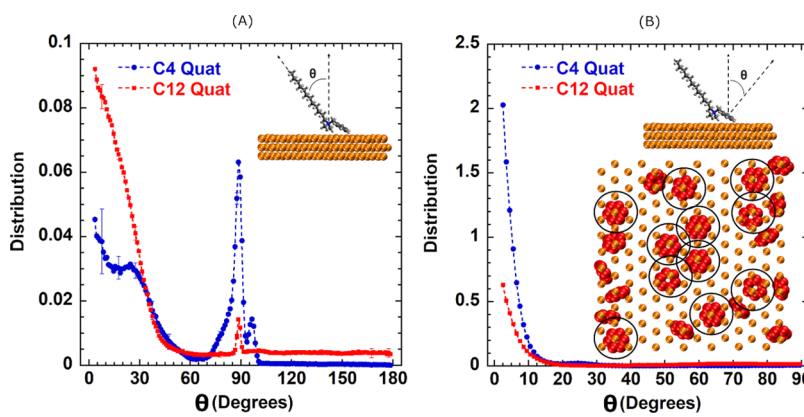


Figure 5. Distribution of orientation of (A) alkyl tails and (B) normal vector of the aromatic rings with respect to the surface normal of adsorbed C4 and C12 molecules. Inset in (B) shows the aromatic rings of C12 Quats that are close to the surface. A good fraction of them lies parallel to the surface. Error bars in (B) are smaller than the size of the markers.

This systematic study will facilitate the design of better corrosion inhibitors for specific corrosive environments. These findings are important for studying liquid–solid interfacial phenomena such as corrosion and for designing better corrosion inhibitors for oil-and-gas transportation pipeline industries.

■ ASSOCIATED CONTENT

SI Supporting Information

The Supporting Information is available free of charge at <https://pubs.acs.org/doi/10.1021/acs.jpclett.0c02517>.

Synthesis and purification Quats, sample preparation, SFG theory, data acquisition, fitting equations and parameters, supporting SFG spectra, peak assignments of C4 and C12 Quats, and MD simulation details ([PDF](#))

■ AUTHOR INFORMATION

Corresponding Author

Katherine Leslee Asetre Cimatu — Department of Chemistry and Biochemistry, Ohio University, Athens, Ohio 45701-2979, United States;  orcid.org/0000-0002-4216-9715; Email: cimatu@ohio.edu

Authors

Md. Rubel Khan — Department of Chemistry and Biochemistry, Ohio University, Athens, Ohio 45701-2979, United States

Himanshu Singh — Department of Chemical and Biomolecular Engineering, Ohio University, Athens, Ohio 45701, United States

Sumit Sharma — Department of Chemical and Biomolecular Engineering, Ohio University, Athens, Ohio 45701, United States;  orcid.org/0000-0003-3138-5487

Complete contact information is available at:

<https://pubs.acs.org/10.1021/acs.jpclett.0c02517>

Notes

The authors declare no competing financial interest.

■ ACKNOWLEDGMENTS

This work is supported by a grant from the National Science Foundation (NSF; CBET-1705817). The authors would like to thank the NSF (CHE-0947031 and CHE-1338000) for the acquisition of the femtosecond laser and nuclear magnetic spectrometer. The authors are thankful to the Department of Chemistry and Biochemistry and the Nanoscale and Quantum Phenomena Institute for financial support. Computational resources for this work were provided by the Ohio Supercomputer Center and National Science Foundation XSEDE (DMR-190005).

■ REFERENCES

- (1) Koch, G. H.; Brongers, M. P. H.; Thompson, N. G.; Virmani, Y. P.; Payer, J. H. *Corrosion Cost and Preventive Strategies in the United States*; NACE International: 2002.
- (2) McMahon, A. J. The Mechanism of Action of an Oleic Imidazoline based Corrosion Inhibitor for Oilfield Use. *Colloids Surf. A* **1991**, *59*, 187–208.
- (3) Popoola, L. T.; Grema, A. S.; Latinwo, G. K.; Gutti, B.; Balogun, A. S. Corrosion Problems During Oil and Gas Production and Its Mitigation. *Int. J. Ind. Chem.* **2013**, *4*, 35.

(4) Kermani, M. B.; Harr, D. In *The Impact of Corrosion on Oil and Gas Industry*; Giornata di Studio IGF S: Donato Milanese, 1996; pp 2008.

(5) Edwards, A.; Osborne, C.; Webster, S.; Klenerman, D.; Joseph, M.; Ostovar, P.; Doyle, M. Mechanistic Studies of the Corrosion Inhibitor Oleic Imidazoline. *Corros. Sci.* **1994**, *36*, 315–325.

(6) Somasundaran, P.; Fuerstennau, D. W. Mechanisms of Alkyl Sulfonate Adsorption at the Alumina-Water Interface. *J. Phys. Chem.* **1966**, *70*, 90–96.

(7) Fan, A.; Somasundaran, P.; Turro, N. J. Adsorption of Alkyltrimethylammonium Bromides on Negatively Charged Alumina. *Langmuir* **1997**, *13*, 506–510.

(8) Jaschke, M.; Butt, H.-J.; Gaub, H. E.; Manne, S. Surfactant Aggregates at a Metal Surface. *Langmuir* **1997**, *13*, 1381–1384.

(9) Orendorff, C. J.; Gole, A. J.; Sau, T. K.; Murphy, C. J. Surface-enhanced Raman Spectroscopy of Self-assembled Monolayers: Sandwich Architecture and Nanoparticle Shape Dependence. *Anal. Chem.* **2005**, *77*, 3261–3266.

(10) Wood, M. H.; Welbourn, R. J. L.; Charlton, T.; Zarbakhsh, A.; Casford, M. T.; Clarke, S. M. Hexadecylamine Adsorption at the Iron Oxide–Oil Interface. *Langmuir* **2013**, *29*, 13735–13742.

(11) Schultz, Z. D.; Biggin, M. E.; White, J. O.; Gewirth, A. A. Infrared-Visible Sum Frequency Generation Investigation of Cu Corrosion Inhibition with Benzotriazole. *Anal. Chem.* **2004**, *76*, 604–609.

(12) Miranda, P. B.; Pflumio, V.; Saito, H.; Shen, Y. R. Surfactant Monolayers at Solid-Liquid Interfaces: Conformation and Interaction. *Thin Solid Films* **1998**, *327*, 161–165.

(13) Harris, A. L.; Chidsey, C. E. D.; Levinos, N. J.; Loiacono, D. N. Monolayer Vibrational Spectroscopy by Infrared-Visible Sum Generation at Metal and Semiconductor Surfaces. *Chem. Phys. Lett.* **1987**, *141*, 350–356.

(14) Zhang, H. P.; Romero, C.; Baldelli, S. Preparation of Akanethiol Monolayers on Mild Steel Surfaces Studied with Sum Frequency Generation and Electrochemistry. *J. Phys. Chem. B* **2005**, *109*, 15520–15530.

(15) Shi, H.; Cai, Z.; Patrow, J.; Zhao, B.; Wang, Y.; Wang, Y.; Benderskii, A.; Dawlaty, J.; Cronin, S. B. Monitoring Local Electric Fields at Electrode Surfaces Using Surface Enhanced Raman Scattering-Based Stark-Shift Spectroscopy during Hydrogen Evolution Reactions. *ACS Appl. Mater. Interfaces* **2018**, *10*, 33678–33683.

(16) Ye, S.; Nihonyanagi, S.; Fujishima, K.; Uosaki, K. Conformational Order of Octadecanethiol (ODT) Monolayer at Gold/Solution Interface: Internal Reflection Sum Frequency Generation (SFG) Study. *Stud. Surf. Sci. Catal.* **2001**, *132*, 705–710.

(17) Cimatu, K. A.; Baldelli, S. Chemical Imaging of Corrosion: Sum Frequency Generation Imaging Microscopy of Gold Surface in Cyanide. *J. Am. Chem. Soc.* **2008**, *130*, 8030–8037.

(18) Wallentine, S.; Bandaranayake, S.; Biswas, S.; Baker, L. R. Plasmon-Resonant Vibrational Sum Frequency Generation of Electrochemical Interfaces: Direct Observation of Carbon Dioxide Electro-reduction on Gold. *J. Phys. Chem. A* **2020**, *124*, 8057–8064.

(19) Cimatu, K.; Baldelli, S. Sum Frequency Generation Microscopy of Microcontact-Printed Mixed Self-Assembled Monolayers. *J. Phys. Chem. B* **2006**, *110*, 1807–1813.

(20) Nonkumwong, J.; Erasquin, U. J.; Sy Piecco, K. W.; Premadasa, U. I.; Aboelenen, A. M.; Tangonan, A.; Chen, J.; Ingram, D.; Srisombat, L.; Cimatu, K. L. A. Successive Surface Reactions on Hydrophilic Silica for Modified Magnetic Nanoparticle Attachment Probed by Sum-Frequency Generation Spectroscopy. *Langmuir* **2018**, *34*, 12680–12693.

(21) Adhikari, N. M.; Premadasa, U. I.; Cimatu, K. L. A. Sum Frequency Generation Vibrational Spectroscopy of Methacrylate-Based Functional Monomers at the Hydrophilic Solid-Liquid Interface. *Phys. Chem. Chem. Phys.* **2017**, *19*, 21818–21828.

(22) Khan, M. R.; Premadasa, U. I.; Cimatu, K. L. A. Role of the Cationic Headgroup to Conformational Changes Undergone by Shorter Alkyl Chain Surfactant and Water Molecules at the Air-Liquid Interface. *J. Colloid Interface Sci.* **2020**, *568*, 221–233.

- (23) Cimatu, K. A.; Chan, S. C.; Jang, J. H.; Hafer, K. Preferential Organization of Methacrylate Monomers and Polymer Thin Films at the Air Interface Using Femtosecond Sum Frequency Generation Spectroscopy. *J. Phys. Chem. C* **2015**, *119*, 25327–25339.
- (24) Cimatu, K. A.; Chan, S. C.; Jang, J. H.; Hafer, K. Preferential Organization of Methacrylate Monomers and Polymer Thin Films at the Air Interface Using Femtosecond Sum Frequency Generation Spectroscopy. *J. Phys. Chem. C* **2015**, *119*, 25327–25339.
- (25) Chan, S. C.; Jang, J. H.; Cimatu, K. A. Orientational Analysis of Interfacial Molecular Groups of a 2-Methoxyethyl Methacrylate Monomer Using Femtosecond Sum Frequency Generation Spectroscopy. *J. Phys. Chem. C* **2016**, *120*, 29358–29373.
- (26) Premadasa, U. I.; Moradighadi, N.; Kotturi, K.; Nonkumwong, J.; Khan, M. R.; Singer, M.; Masson, E.; Cimatu, K. L. A. Solvent Isotopic Effects on a Surfactant Headgroup at the Air–Liquid Interface. *J. Phys. Chem. C* **2018**, *122*, 16079–16085.
- (27) Adhikari, N. M.; Premadasa, U. I.; Rudy, Z. J.; Cimatu, K. L. A. Orientational Analysis of Monolayers at Low Surface Concentrations Due to an Increased Signal-to-Noise Ratio (S/N) Using Broadband Sum Frequency Generation Vibrational Spectroscopy. *Appl. Spectrosc.* **2019**, *73*, 1146–1159.
- (28) Wang, W.; Ye, S. Molecular Interactions of Organic Molecules at the Air/Water Interface Investigated by Sum Frequency Generation Vibrational Spectroscopy. *Phys. Chem. Chem. Phys.* **2017**, *19*, 4488–4493.
- (29) Nishi, N.; Hobara, D.; Yamamoto, M.; Kakiuchi, T. Total-Internal-Reflection Broad-Bandwidth Sum Frequency Generation Spectroscopy of Hexadecanethiol Adsorbed on Thin Gold Film Deposited on CaF₂. *Anal. Sci.* **2003**, *19*, 887–890.
- (30) Quast, A. D.; Wilde, N. C.; Matthews, S. S.; Maughan, S. T.; Castle, S. L.; Patterson, J. E. Improved Assignment of Vibrational Modes in Sum-Frequency Spectra in the CH Stretch Region for Surface-Bound C18 Alkylsilanes. *Vib. Spectrosc.* **2012**, *61*, 17–24.
- (31) Richter, L. J.; Petrali-Mallow, T. P.; Stephenson, J. C. vibrationally Resolved Sum-Frequency Generation with Broad-Bandwidth Infrared Pulses. *Opt. Lett.* **1998**, *23*, 1594–1596.
- (32) Verreault, D.; Kurz, V.; Howell, C.; Koelsch, P. Sample Cells for Probing Solid/Liquid Interfaces with Broadband Sum-Frequency-Generation Spectroscopy. *Rev. Sci. Instrum.* **2010**, *81*, 063111.
- (33) Ma, G.; Allen, H. C. Surface Studies of Aqueous Methanol Solutions by Vibrational Broad Bandwidth Sum Frequency Generation Spectroscopy. *J. Phys. Chem. B* **2003**, *107*, 6343–6349.
- (34) Premadasa, U. I.; Adhikari, N. M.; Cimatu, K. L. A. Molecular Insights into the Role of Electronic Substituents on the Chemical Environment of the –CH₃ and >C=O Groups of Neat Liquid Monomers Using Sum Frequency Generation Spectroscopy. *J. Phys. Chem. C* **2019**, *123*, 28201–28209.
- (35) Malyk, S.; Shalhout, F. Y.; O’Leary, L. E.; Lewis, N. S.; Benderskii, A. V. Vibrational Sum Frequency Spectroscopic Investigation of the Azimuthal Anisotropy and Rotational Dynamics of Methyl-Terminated Silicon(111) Surfaces. *J. Phys. Chem. C* **2013**, *117*, 935–944.
- (36) Vericat, C.; Vela, M. E.; Benitez, G.; Carro, P.; Salvarezza, R. C. Self-Assembled Monolayers of Thiols and Dithiols on Gold: New Challenges for a Well-Known System. *Chem. Soc. Rev.* **2010**, *39*, 1805–1834.
- (37) Miranda, P. B.; Pflumio, V.; Saijo, H.; Shen, Y. R. Surfactant Monolayers at Solid–Liquid Interfaces: Conformation and Interaction. *Thin Solid Films* **1998**, *327–329*, 161–165.
- (38) Premadasa, U. I.; Adhikari, N. M.; Baral, S.; Aboelenen, A. M.; Cimatu, K. L. A. Conformational Changes of Methacrylate-Based Monomers at the Air–Liquid Interface Due to Bulky Substituents. *J. Phys. Chem. C* **2017**, *121*, 16888–16902.
- (39) Chan, S. C.; Jang, J. H.; Cimatu, K. A. Orientational Analysis of Interfacial Molecular Groups of a 2-Methoxyethyl Methacrylate Monomer Using Femtosecond Sum Frequency Generation Spectroscopy. *J. Phys. Chem. C* **2016**, *120*, 29358–29373.
- (40) Meena, S. K.; Sulpizi, M. Understanding the Microscopic Origin of Gold Nanoparticle Anisotropic Growth from Molecular Dynamics Simulations. *Langmuir* **2013**, *29*, 14954–14961.
- (41) da Silva, J. A.; Meneghetti, M. R. New Aspects of the Gold Nanorod Formation Mechanism via Seed-Mediated Methods Revealed by Molecular Dynamics Simulations. *Langmuir* **2018**, *34*, 366–375.
- (42) Patel, A. J.; Varilly, P.; Chandler, D. Fluctuations of Water Near Extended Hydrophobic and Hydrophilic Surfaces. *J. Phys. Chem. B* **2010**, *114*, 1632–1637.